Int. J. Heat Mass Transfer. Vol. 13, pp. 1133–1152. Pergamon Press 1970. Printed in Great Britain

AXIAL STABILITY OF THE DRY PATCH FORMED IN DRYOUT OF A TWO-PHASE ANNULAR FLOW

G. D. McPHERSON

Advance Engineering Branch, Chalk River Nuclear Laboratories, Atomic Energy of Canada Limited, Chalk River, Ontario, Canada

(*Received* 9 *September* 1969 *and in revised form* 19 *December* 1969)

Abstract— In cooling nuclear fuel by two-phase water–steam mixtures, the formation of a dry patch (dryout) on the fuel can lead to unacceptably high sheath and fuel temperatures. Dryout is initiated by nucleation or thermocapillary forces in the liquid film which normally flows over the heated surface or by film starvation. Depending on the force balance at the upstream vertex or stagnation point of the dry patch, the patch may be quasi-stable or transient, growing upstream or rewetting.

The forces considered are:

- thrust of the vapour leaving the film surface
- stagnation or deceleration force on the film upstream of the stagnation point
- surface tension in the neighbourhood of the stagnation point
- vapour shear at the film–vapour interface
- hydrostatic head from the liquid film
- drag at the small step in the film.

The distance upstream of the dry patch boundary over which these forces are effective is divided into that distance over which the film is being decelerated and diverted with no change in thickness, and that distance over which evaporation reduces the thickness to zero. The following details are taken into account in the analysis:

- film velocity profile
- reduction in the stagnation force due to the evaporative flow
- temperature and heat flux distributions over the heater surface and across the film
- film shape.

The forces are evaluated for typical dryout conditions. Interpretations of the results suggests that for dry patch stability, the shear force must equal the surface force. Mechanisms are proposed whereby these forces can maintain a quasi-stable balance. Comparisons are made with a similar approach by Zuber and some important differences are noted.

NOMENCLATURE

a, b, constants relating heat flux and liquid film thickness;

d_e, equivalent diameter of the wetted perimeter used in calculation of F_D [ft];

F, resultant axial force per ft width on liquid film at vertex of dry patch [lb/ft];

F_B, axial body force per ft width on liquid film at vertex of dry patch [lb/ft];

F_D, axial drag force per ft width on liquid film at vertex of dry patch [lb/ft];

F_E, axial vapour thrust force per ft width on liquid film at vertex of dry patch [lb/ft];

F_M, axial stagnation force per ft width on liquid film at vertex of dry patch [lb/ft];

F_S, axial shear force per ft width on liquid film at vertex of dry patch [lb/ft];

F_γ, axial surface force per ft width on liquid film at vertex of dry patch [lb/ft];

g, acceleration due to gravity [ft/h^2];

g_c, conversion factor [lb_m . ft/h^2 . lb_f];

k, Prüger's constant [ft/h . psi];

l, characteristic distance between vertex of dry patch and the undisturbed liquid

m, characteristic distance between vertex of dry patch and the point upstream

where the film thickness begins to decrease due to evaporation [ft];
p, pressure [psia];
$\dot{Q}/A$, heat flux [Btu/h . ft^2];
T, temperature [°F];
u, axial velocity component in downstream direction [ft/h];
v_G, vapour velocity normal to liquid–vapour interface [ft/h];
v_L, Prüger's interfacial "sinking velocity" due to evaporation [ft/h];
y, film depth measured perpendicular to heater surface [ft].

Greek symbols

γ, surface tension at the liquid–vapour interface [lb/ft];
δ, liquid film thickness [ft];
θ, contact angle;
λ, latent heat of vaporization [Btu/lb];
ρ, density [lb/ft^3];
ϕ_E, effective contact angle at equilibrium;
φ, angle of surface roughness or liquid–vapour interface relative to axis;
τ, shear stress [lb/ft^2].

Subscripts

A, advancing liquid film;
E, over the evaporating length, or in the case of contact angles effective equilibrium value;
G, vapour;
i, at the liquid–vapour interface;
L, liquid;
max, maximum value;
o, at the liquid–wall interface;
R, receding liquid film;
sat, saturation value;
∞, in the undisturbed film upstream of the dry patch.

1. INTRODUCTION

At qualities above 10–20 per cent a water–steam mixture flowing in a heated channel flows in an annular or annular-dispersed pattern: a portion of the liquid flows as a film on the channel walls and the remainder is carried in the vapour core. As the coolant quality is raised the liquid film eventually breaks down. At qualities approaching 100 per cent this may be due to a lack of liquid to replenish the evaporating film. At lower qualities it may be caused by a thermodynamic or hydrodynamic phenomenon such as nucleation in the liquid film, a local thinning of the film or a local diversion of the normal deposition from the core to the film.

When the film breaks down at lower qualities a dry patch forms on the heated wall. Rewetting depends on the temperature to which the patch rises while it is dry and on the forces acting on the film at the boundary. The temperature effect was studied with an analogue technique reported in [1] where it was shown that the dry surface temperature may exceed the Leidenfrost value and that although conditions may change to produce a resultant downstream force on the film boundary the film will not immediately rewet the patch. The objective in this paper is to examine the forces acting on the film and define conditions for which the film boundary will tend to recover the patch, remain stable or move upstream.

2. FORCES ACTING ON THE UPSTREAM BOUNDARY OF A DRY PATCH

2.1 *Review*

Hartley and Murgatroyd presented the first treatment of a dry patch in adiabatic flow [2]. They considered a patch of the shape shown in Fig. 1 and assumed that the liquid in the central stream segment AB stagnates and the flow follows the stream lines shown in the plan view. For dry patch stability they equated the upstream forces on AB due to the liquid–vapour surface force, γ, and given by $\gamma(1 - \cos\theta)$* to that force required to bring the liquid in AB to rest from its velocity in the undisturbed film at A. Subsequently, Hewitt and Lacey reported experiments on dry patch stability in which the

* Thus they made the reasonable assumption that the curvature of the stream around the dry patch is much less than that of the meniscus.

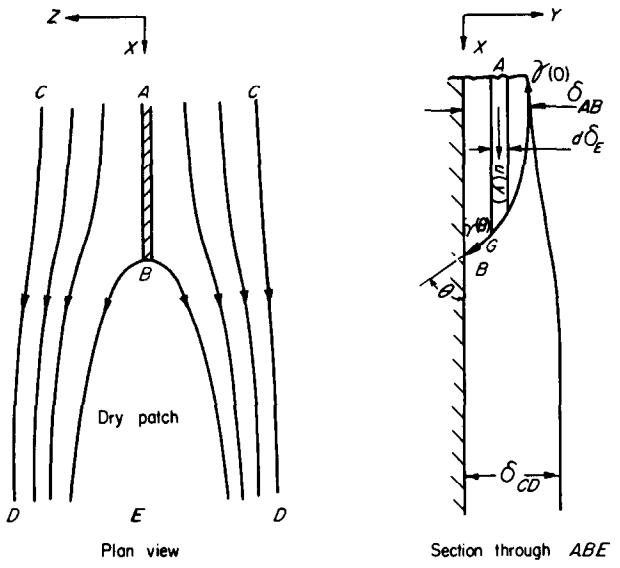

FIG. 1. Model of flow around dry patch by Hartley and Murgatroyd [2].

static contact angle was measured [3]. Applying Hartley and Murgatroyd's force balance they found the upstream surface tension force was about eight times the force required to bring the film to rest. To explain this discrepancy they suggested an aerodynamic force on the bulge which had been observed immediately upstream of dry patches in adiabatic flow.

Murgatroyd called this a form force and for forced convective flow proposed an additional shear force [4]. The latter is the resultant of the vapour–liquid shear, τ_i, which changes very little towards the stagnation point, and the wall shear, τ_0, which decreases gradually as the film stagnates (Fig. 2). He defined the shear force by the expression $\lambda\tau_i$ where λ is a characteristic

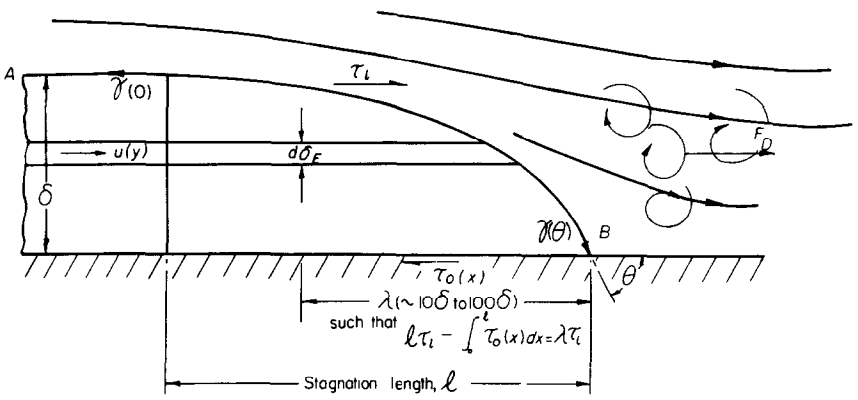

FIG. 2. Forces on liquid film upstream of dry patch in adiabatic flow, by Murgatroyd [4].

length which probably lies in the range 10–100 δ, and δ is the undisturbed film thickness. The form force, F_D, is also expressed in terms of τ_i. From the analysis of experimental results for flow over transverse cylindrical bodies and steps F_D is shown to lie in the range 10 $\delta\tau_i$ to 25 $\delta\tau_i$.

Using the data from [3] and assuming that the static and dynamic contact angles are equal, Murgatroyd found that the resultant of these shear and form forces was about twenty times that due to the film momentum. More information is required on the dynamic contact angle and the magnitudes of these two new forces to verify this conclusion.

Staub and Zuber were first to consider dry patch stability over a heated surface in [5] and later in [6]. They included Hartley and Murgatroyd's forces due to stagnation pressure and surface tension and added two new ones: the non-uniform surface tension over the meniscus due to a variation in the film temperature and the thrust on the film due to evaporation from the meniscus. This approach is discussed in detail later where it is compared with my approach which follows:

2.2 *Assumptions*

Consider the thin film in uniform shear motion over a horizontal flat heated surface (Fig. 3). I assume deposition, entrainment and evaporation over the undisturbed film are in equilibrium and the resulting rate of mass transfer does not disrupt the film velocity profile. Let the profile be linear and defined by

$$u_L(y) = \frac{y}{\delta} \cdot u_{Li} = \frac{2\bar{u}_L y}{\delta} \tag{1}$$

where u_{Li} is the film velocity at the liquid–vapour interface and the other symbols are explained in Fig. 3. This is a good approximation as demonstrated experimentally in [1].

At some point on the heated surface a dry patch is formed in the film. Let $\bar{u}_{L\infty}$ be the mean velocity of the undisturbed film upstream of the dry patch. Due to low heat transfer rates from the patch to the vapour core the patch temperature rises and heat is conducted along the sheath from the patch to the film. Thus there is an increase in the heat flux across the film surrounding the dry patch. This causes an increased evaporation rate from the film in the region defined by the distance m. In [1] McPherson and Murgatroyd show that m is much smaller than the dry patch width, hence, it is reasonable to assume that none of the liquid within this distance passes around the patch but must all evaporate. Due to the deviation of some of the liquid around the patch the mean film velocity at m will be reduced to some value $\bar{u}_{LE}$. I assume that upstream of m the film thickness remains constant and downstream of m the velocity profile is identical to that at m, i.e. when the higher velocity surface liquid is evaporated, there is insufficient time for the thinning film to be accelerated to equilibrium.

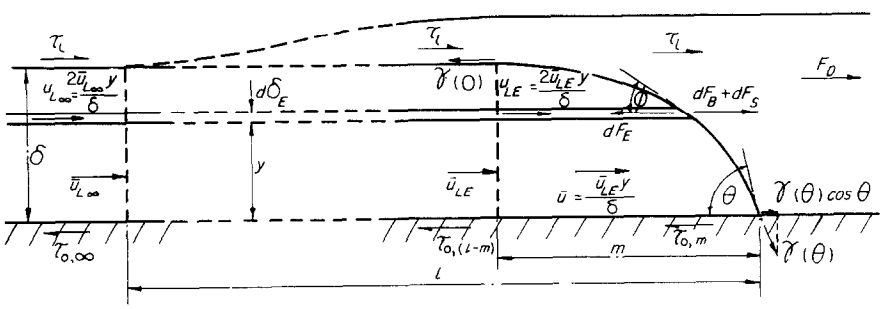

FIG. 3. Cross-section through central stream segment of liquid film upstream of dry patch.

As shown in Fig. 3, I propose that the resultant force acting on the liquid at the vertex of the dry patch is the sum of the following forces: the vapour thrust, F_E, the stagnation force, F_M, the shear force, F_S, the surface force, F_γ, the body force, F_B, and the drag force, F_D. My analysis of each force follows.

2.3 *The vapour thrust*

There is an axial component of vapour thrust on the film where its thickness is reduced to zero by evaporation. Consider a segment of the film, $d\delta_E$, at a distance y from the wall (Fig. 4).

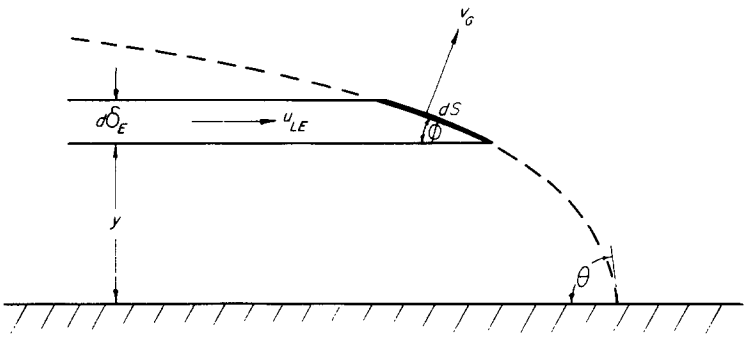

FIG. 4. Vapour thrust over central stream segment of liquid film upstream of dry patch.

To separate the effect of momentum due to the film velocity u_{LE} from the resultant vapour momentum, consider the case $u_{LE} = 0$. The resultant vapour velocity then is $v_G \perp dS$. The axial component of the vapour thrust on dS would be given by the product of the mass flow rate through dS, $\rho_G v_G dS/g_c$, times the axial component of the vapour velocity $u_G = v_G \sin\varphi$,

$$\text{viz. } dF_E = -\frac{\rho_G v_G^2 \sin\varphi\, dS}{g_c} = -\frac{\rho_G v_G^2\, d\delta_E}{g_c}. \quad (2)$$

Since the liquid is actually flowing with constant velocity, u_{LE}, it has an associated momentum which must be conserved in the vapour. This component remains unchanged over the interface and does not affect the force balance.

Since the total liquid flow in m is evaporating, the mass flow rate through dS must equal the evaporation rate due to the heat flux from the projected area of dS on the heater wall,

$$\text{i.e.} \quad \frac{\rho_G v_G\, d\delta_E}{g_c \sin\varphi} = \frac{\dot{Q}/A \cot\varphi d\delta_E}{\lambda g_c}$$

$$\therefore \quad v_G = \frac{\dot{Q}/A}{\rho_G \lambda}\cos\varphi$$

where λ is the latent heat of vaporization. Substitution of this expression in (2) gives

$$dF_E = -\frac{(\dot{Q}/A)^2 \cos^2\varphi\, d\delta_E}{g_c \rho_G \lambda^2}.$$

Hence

$$F_E = \frac{1}{g_c \rho_G \lambda^2}\int_0^\delta (\dot{Q}/A)^2 \cos^2\varphi\, d\delta_E. \quad (3)$$

A heat flux of $\dot{Q}/A$ will cause a change in film thickness $d\delta_E$ over heater length dx given by

$$d\delta_E = -\frac{(\dot{Q}/A)\, dx}{u_{LE}\rho_L \lambda} \quad (4)$$

where u_{LE} is the axial velocity of that portion of the film in $d\delta_E$. Since the velocity profile is assumed linear then downstream of m

$$u_{LE} = \frac{2\bar{u}_{LE} y}{\delta} \quad (5)$$

where $\bar{u}_{LE}$ is the mean film velocity at m. At the

film surface this becomes:

$$u_{LE} = \frac{2\bar{u}_{LE}\delta_E}{\delta}.$$

Hence (4) can be written in terms of the slope of the liquid surface:

$$\tan\varphi = \frac{d\delta_E}{dx} = -\frac{(\dot{Q}/A)\,\delta}{2\bar{u}_{LE}\rho_L\lambda\delta_E}. \quad (6)$$

Figure 5 may be constructed from (6) and cos φ calculated for substitution in (3) later.

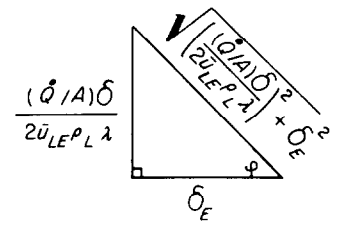

FIG. 5. Representation of equation (6) to calculate cos φ.

2.4 *The stagnation force*

In 2.2 I assumed that any liquid reaching m will cease to be decelerated and continue on to evaporate. Therefore the stagnation term will involve the momentum change between l and m, i.e.

$$F_M = \int_0^{\delta}\int_{u_{LE}}^{u_{L\infty}} \frac{\rho_L u\,du\,d\delta_E}{g_c}$$

$$= \frac{\rho_L}{2g_c}\int_0^{\delta}(u_{L\infty}^2 - u_{LE}^2)\,d\delta_E. \quad (7)$$

Substituting from (1)

$$F_M = \frac{\rho_L}{2g_c}\int_0^{\delta}\left[\left(\frac{2\bar{u}_{L\infty}y}{\delta}\right)^2 - \left(\frac{2\bar{u}_{LE}y}{\delta}\right)^2\right]d\delta_E$$

$$F_M = \frac{2\rho_L\delta}{3g_c}(\bar{u}_{L\infty}^2 - \bar{u}_{LE}^2) \quad (8)$$

which gives the axial stagnation force over the meniscus due to the deceleration of the film. This term becomes zero for $\bar{u}_{LE} = \bar{u}_{L\infty}$, the case when the heat flux is sufficient to evaporate all the liquid in the film and none is diverted around the patch.

2.5 *The shear force*

This is the resultant of the interfacial shear τ_i and the surface shear τ_0. τ_i remains constant over l while τ_0 decreases due to a restraining force at the vertex of the dry patch. In the undisturbed film beyond l,

$$\tau_{0\infty} = -\tau_i. \quad (9)$$

Between l and m the mean film velocity decreases from $\bar{u}_{L\infty}$ to $\bar{u}_{LE}$. Assuming the deceleration is linear over this distance the mean film velocity is

$$\bar{u}_L = \bar{u}_{LE} + \frac{m+x}{m-l}(\bar{u}_{L\infty} - \bar{u}_{LE}), \quad -l \geqslant x \geqslant -m. \quad (10)$$

For a linear velocity profile in a film of given thickness

$$\frac{du}{dy} \propto \bar{u}_L.$$

Therefore

$$\tau_0 \propto \bar{u}_L$$

and

$$\tau_{0\infty} \propto \bar{u}_{L\infty}.$$

Hence

$$\tau_0 = \tau_{0\infty}\frac{\bar{u}_L}{\bar{u}_{L\infty}}$$

and from (9)

$$\tau_0 = -\tau_i\frac{\bar{u}_L}{\bar{u}_{L\infty}}.$$

The resultant shear force on the film over the deceleration distance $l - m$ is

$$F_{S.(l-m)} = \tau_i(l-m) - \int_{-l}^{-m}\tau_i\frac{\bar{u}_L}{\bar{u}_{L\infty}}\,dx.$$

Substituting $\bar{u}_L$ from (10) and integrating,

$$F_{S.(l-m)} = \frac{\tau_i |l-m|}{2}\left(1 - \frac{\bar{u}_{LE}}{\bar{u}_{L\infty}}\right). \quad (11)$$

Over the distance from $-m$ to 0 the film velocity profile remains unchanged. By the previous argument, the shear differential over m is constant at

$$\tau_i - \tau_i \frac{\bar{u}_{LE}}{\bar{u}_{L\infty}}.$$

Hence the differential shear force is

$$F_{S.(m-0)} = \tau_i m\left(1 - \frac{\bar{u}_{LE}}{\bar{u}_{L\infty}}\right). \quad (12)$$

Adding equations (11) and (12) the resultant shear force is

$$F_S = \tau_i \left(\frac{l+m}{2}\right)\left(1 - \frac{\bar{u}_{LE}}{\bar{u}_{L\infty}}\right). \quad (13)$$

2.6 *The surface force*

Prüger [7] and Jakob [8] have shown that the surface temperature of a liquid film supporting an evaporative heat flux exceeds saturation by an amount proportional to the heat flux. McPherson and Murgatroyd [1] found a variation in heat flux over the film meniscus upstream of the dry patch. Therefore the magnitude of γ varies over the meniscus and is given by (Fig. 3)

$$F_\gamma = \gamma(\theta)\cos\theta - \gamma(0). \quad (14)$$

2.7 *The body force*

The downstream force on the meniscus due to the weight of the film is

$$F_B = \int_0^\delta \frac{\rho_L g y \, d\delta_E}{g_c} = \frac{\rho_L g \delta^2}{2g_c}. \quad (15)$$

2.8 *The drag force*

Murgatroyd [4] gave the following analysis of the drag or form force which results when the vapour flows over the disturbing step of the vertex: Wieghardt [9] reported such a study in terms of a friction factor based on the step area and the free stream dynamic head, i.e. $\frac{1}{2}\rho_G \bar{u}_G^2 \delta$. In the appendix to [4], Hartley re-analyzed Weighardt's data in terms of a friction factor based on the average local dynamic head in the boundary layer up to the height of the step,

i.e. $$\frac{\rho_G}{2}\int_0^\delta u_G^2 \, d\delta_E.$$

Over the full range of step heights observed (from 3·6 to 48 per cent of the boundary layer thickness) the drag coefficient resulting from this new analysis was found approximately constant at 0·20. Hence the drag force in the step within the vapour boundary layer can be expressed by

$$F_D = 0{\cdot}2\int_0^\delta \tfrac{1}{2}\rho_G u_G^2 \, d\delta_E. \quad (16)$$

Hartley found it useful to express this in the form

$$F_D = k\tau_i \delta. \quad (17)$$

He assumed a 1/7th power law gas velocity distribution, solved (16) and arranged the result of (17). I use the resulting equation,

$$F_D = \left(0{\cdot}416\frac{\delta}{d_e}\right)^{\frac{1}{4}}\tau_i \delta \quad (18)$$

where d_e is the equivalent diameter of the wetted perimeter.

2.9 *The force balance for linear and constant velocity profiles*

The resultant axial force acting on the central stream segment of liquid film upstream of a dry patch with heat transfer is

$$F = F_E + F_M + F_S + F_\gamma + F_B + F_D$$

which, from equations (3), (8), (13)–(15) and (18), is

$$F = \frac{1}{g_c \rho_G \lambda^2} \int_0^{\delta} (\dot{Q}/A)^2 \cos^2 \varphi \mathrm{d}\delta_E + \frac{2\rho_L \delta}{3g_c}(\bar{u}_{L\infty}^2 - \bar{u}_{LE}^2) + \tau_i \frac{(l+m)}{2}\left(1 - \frac{\bar{u}_{LE}}{\bar{u}_{L\infty}}\right) + [\gamma(\theta)\cos\theta - \gamma(0)] + \frac{\rho_L g \delta^2}{2g_c} + \left(0{\cdot}416\frac{\delta}{d_e}\right)^{\frac{1}{7}} \tau_i \delta. \quad (19)$$

It is interesting to consider the case where the mass transfer between liquid film and vapour core is so great that the equilibrium velocity profile is completely disrupted. As a limiting case, it can be represented by a constant, $\bar{u}_{LE}$, and the force equation becomes:

In every case the stability conditions are as follows:

$F = 0$: stable dry patch
$F > 0$: film recovers
$F < 0$: dry patch grows upstream.

$$F = \frac{1}{g_c \rho_G \lambda^2} \int_0^{\delta} (\dot{Q}/A)^2 \cos^2 \varphi \mathrm{d}\delta_E + \frac{\rho_L \delta}{2g_c}(\bar{u}_{L\infty}^2 - \bar{u}_{LE}^2) + \tau_i \frac{(l+m)}{2}\left(1 - \frac{\bar{u}_{LE}}{\bar{u}_{L\infty}}\right) + [\gamma(\theta)\cos\theta - \gamma(0)] + \frac{\rho_L g \delta^2}{2g_c} + \left(0{\cdot}416\frac{\delta}{d_e}\right)^{\frac{1}{7}} \tau_i \delta \quad (20)$$

where $\cos\varphi$ is evaluated from (4) rather than (6). Later the magnitudes of the forces resulting from these two velocity profiles will be compared.

The combination of a low heat-transfer coefficient to steam, h_G, and low axial conduction in the heater wall may result in a heat flux at the patch boundary which completely evaporates the film as it arrives. To represent this condition $\bar{u}_{LE}$ is set equal to $\bar{u}_{L\infty}$ in the force equation. In both the linear and the constant film velocity profile cases,

$$F = \frac{1}{g_c \rho_G \lambda^2} \int_0^{\delta} (\dot{Q}/A)^2 \cos^2 \varphi \, \mathrm{d}\delta_E + [\gamma(\theta)\cos\theta - \gamma(0)] + \frac{\rho_L g \delta^2}{2g_c} + \left(0{\cdot}416\frac{\delta}{d_e}\right)^{\frac{1}{7}} \tau_i \delta \quad (21)$$

3. APPLICATION OF THE FORCE BALANCE TO DRYOUT CONDITIONS

3.1 *The shape of the meniscus and the associated heat flux distribution*

Dryout is known to have occurred in a Harwell test section consisting of an electrically heated tube at these conditions:

two-phase annular flow, 85 per cent quality;
0·497 in. dia. stainless steel tube, 0·064 in. wall thickness;
mass flux, $0{\cdot}5 \times 10^6$ lb/h ft^2;
pressure, 1000 psia;
heat flux, 200 000 Btu/h ft^2;
vapour heat-transfer coefficient,* 667 Btu/h ft^2 °F;
film heat-transfer coefficient,* 20 000 Btu/h ft^2 °F;

* Evaluated from equations (9) and (10) of [10].

film thickness on approach to dry patch* 4·9 μ = 0·000016 ft.

I have estimated the film shape immediately upstream of the dry patch using a resistance paper analogue technique described in [1]. The paper is cut out to represent the dry patch, the heater sheath and the cross-section through the central stream segment of film upstream of the dry patch; dimensions are chosen to simulate thermal resistance and electric potentials are applied to represent heat input. The resulting potential field represents the temperature field and electric current represents the heat flux. The technique involves measuring the heat flux through different segments of the simulated film upstream of the dry patch and adjusting the film thickness, δ_E, by an amount equivalent to the evaporation rate caused by the heat flux.

I considered stainless steel walls 0·032 in., 0·041 in. and 0·064 in. thick at the dryout con-

1 ft/s and 2 ft/s constant profile and 1 ft/s linear profile.†

Solutions of film thickness are tabulated in Table 1 and plotted in Fig. 6. Note that the slope of the interface is very gradual beyond 0·1 mm and lies in the range 1/200–1/400; as expected the higher velocity film has the more gradual slope.

Film thickness vs. heat flux‡ is plotted in Fig. 7 for the five cases considered. Generally the curves show a logarithmic relationship of the form

$$\dot{Q}/A = a\delta_E^{-b}. \tag{22}$$

The curves have been fitted visually; the resulting constants, a and b, are given in Table 2.

Equation (3) can now be solved for vapour thrust.

3.2 *Solution of the vapour thrust expression*

For the case of a linear velocity profile, from Fig. 5,

$$\cos^2\varphi = \frac{\delta_E^2}{[(\dot{Q}/A)\delta/2\bar{u}_{LE}\rho_L\lambda]^2 + \delta_E^2}. \tag{23}$$

Substituting (22) and (23) in the expression for vapour thrust, (3),

$$F_E = \frac{1}{g_c\rho_G\lambda} \times \int_0^{\delta} \frac{a^2\delta_E^{2(1-b)}}{(a\delta_E^{-b}\delta/2\bar{u}_{LE}\rho_L\lambda)^2 + \delta_E^2}\,\mathrm{d}\delta_E$$

hence

$$F_E = \frac{a^2}{g_c\rho_G\lambda^2} \times \left[\frac{\delta^{1-2b}}{1-2b} + \frac{a^2\delta^{1-4b}}{(4b+1)(2\bar{u}_{LE}\rho_L\lambda)^2}\right]. \tag{24}$$

Similarly $\cos^2\varphi$ can be evaluated from (4) to give the vapour thrust for the case of a constant velocity profile:

$$F_E = \frac{a^2}{g_c\rho_G\lambda^2} \times \left[\frac{\delta^{1-2b}}{1-2b} + \frac{a^2\delta^{1-4b}}{(4b-1)(\bar{u}_{LE}\rho_L\lambda)^2}\right]. \tag{25}$$

3.3 *Solution of the surface force expression*

From Section 2.6

$$F_\gamma = \gamma(\theta)\cos\theta - \gamma(0). \tag{14}$$

To evaluate $\gamma(0)$, we refer to [7] in which Prüger has experimentally determined the temperature rise above saturation at an evaporating liquid surface in terms of the liquid sinking velocity v_L. He expressed the relationship in

* Assuming laminar flow and heat transfer by conduction through the film.

† For the linear profile case the expression for the change in film thickness due to evaporation, equation (4) of [1], was modified by replacing $\bar{u}_{LE}$ with $u_{LE} = 2y\bar{u}_{LE}/\delta$. The heater walls of 0·032 in. and 0·041 in. differ from the 0·064 in. wall in the Harwell experiment, but have been included to provide comparisons.

‡ The surface temperature distributions from which heat flux is calculated are reported in [1] and [11] and some are plotted in Figs. 10 and 11 of this paper.

Table 1. Thickness of evaporating film on approach to triple interface

Wall thickness	Liquid film thickness δ_E (μ)				
	41 mil SS	32 mil SS		64 mil SS	
Axial position relative to triple interface (mils)	Linear velocity profile $\bar{u}_{LE} = \frac{2y\bar{u}_{LE}}{\delta}$ (ft/s)	Constant velocity profile $\bar{u}_{LE} = 1$ ft/s			Constant velocity profile $\bar{u}_{LE} = 2$ ft/s
0	0	0	0	0	0
−0·074	1·48	0·660	0·615	0·773	0·484
−0·147	1·98	0·883	0·787	1·06	0·673
−0·221	2·24	1·02	0·935	1·25	0·800
−0·294	2·37	1·17	1·08	1·41	0·920
−0·368	2·48	1·29	1·20	1·53	1·03
−0·735	2·95	1·84	1·70	2·18	1·39
−1·10	3·30	2·25	2·10	2·62	1·66
−1·47	3·58	2·62	2·47	3·00	1·93
−1·84	3·83	2·94	2·77	3·36	2·14
−2·21	4·03	3·25	3·06	3·72	2·35
−2·58	4·24	3·60	—	—	—
−2·94	4·41	3·93	—	—	—

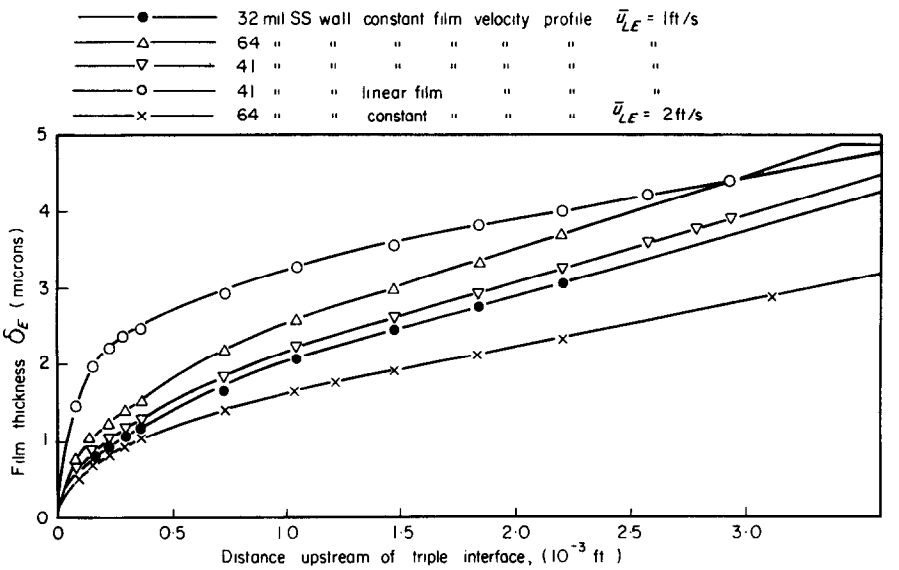

FIG. 6. Thickness of central stream segment of evaporating film upstream of dry patch.

terms of the pressure increase above saturation, $k \cong 1{\cdot}65$ ft/h lb/in^2.

$$\Delta p = v_L/k \qquad (26)$$

From a heat balance

$$v_L = \frac{\dot{Q}/A}{\rho_L \lambda},$$

where

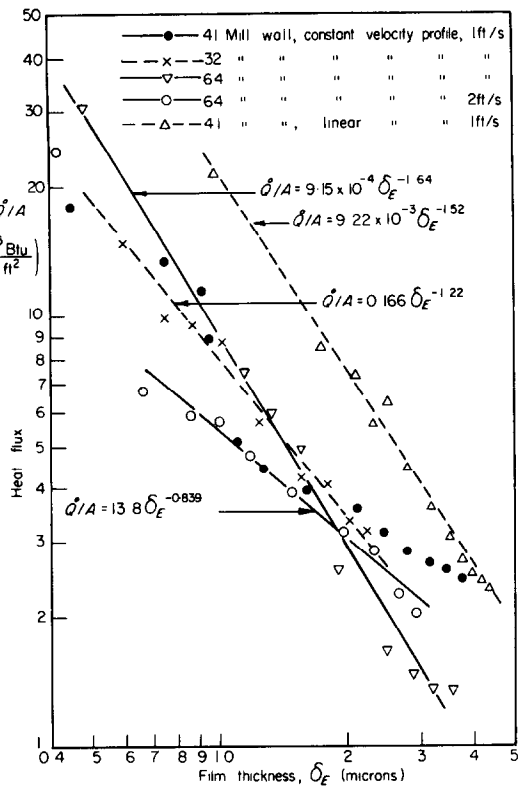

FIG. 7. Heat flux vs. film thickness for various wall thicknesses and film velocities.

Hence the local surface pressure, p, given by (26) is

$$p = p_{sat} + \frac{\dot{Q}/A}{k\rho_L\lambda} \tag{27}$$

and $\gamma(0)$ is the liquid–vapour surface tension at the saturation temperature corresponding to p.

It is difficult to estimate $\gamma(\theta)$ because the heat flux at the triple interface reaches an indeterminable value. In the limit if the pressure at this point exceeds the critical pressure $\gamma(\theta)$ will be zero. However I have estimated the temperature at this point using resistance paper analogues for a variety of cases. The results are described in the Appendix and in Fig. 11 this temperature is shown to lie between 48 and 100°F above saturation. Therefore I assume the average of these two limits, 74°F, for the case in question ($\dot{Q}/A = 200\,000$ Btu/hft^2). In applying this analysis to other cases this temperature should be adjusted in direct proportion to the average heat flux.

3.4 *Evaluation of the force equations*

3.4.1 *Case* $\bar{u}_{LE} = \bar{u}_{L\infty}$. The heat flux is adequate to evaporate the film as it arrives. From

Table 2. Comparison of forces on the meniscus of a liquid film of constant or linear velocity profiles, assuming $\bar{u}_{LE} = \bar{u}_{L_\infty}$

Case	1	2	3	4	5
Velocity profile	constant	constant	constant	constant	linear
$\bar{u}_{L_\infty}$ (ft/s)	1	2	1	1	1
Wall thickness (mil)	64	64	32	41	41
$a \times 10^3$	0·915	166	13 800	0·915	9·22
b	1·640	1·226	0·839	1·640	1·523
Thrust, F_E (10^{-10} lb/ft)	−1·3	−6·1	−17·8	−1·3	−9·6
Surface, F_γ (10^{-5} lb/ft)	− (125 − 61 cos θ)	−6·2	−17·8	−1·3	−9·6
Body, F_B (10^{-10} lb/ft)	59	−6·2	−17·8	−1·3	−9·6
Drag, F_D (10^{-10} lb/ft)	370	−6·2	−17·8	−1·3	−9·6

Physical properties and flow parameters at 1000 psia used in solution of (28) and (29):

$\lambda = 650$ Btu/lb
$\gamma = 0{\cdot}00125$ lb/ft
$\rho_G = 2{\cdot}234$ lb/ft^3
$\rho_L = 46{\cdot}3$ lb/ft^3
$d_e = 0{\cdot}0414$ ft (from Harwell experiment)
$\tau_i = 0{\cdot}364$ lb/ft^2 (from Blasius friction factor, for $\bar{u}_{L\infty} = 2$ ft/s
$= 0{\cdot}182$ lb/ft^2 (for $\bar{u}_{L\infty} = 1$ ft/s)

(21) and (24) the force equation is

$$F = \frac{a^2}{g_c \rho_G \lambda^2}\left[\frac{\delta^{1-2b}}{1-2b} + \frac{a^2\delta^{1-4b}}{(4b+1)(2\bar{u}_{L\infty}\rho_L\lambda)^2}\right] + [\gamma(\theta)\cos\theta - \gamma(0)] + \frac{\rho_L g\delta^2}{2g_c} + \left(0{\cdot}416\frac{\delta}{d_e}\right)^{\frac{1}{2}}\tau_i\delta \qquad (28)$$

for the linear velocity profile.

From (21) and (25),

$$F = \frac{a^2}{g_c \rho_G \lambda^2}\left[\frac{\delta^{1-2b}}{1-2b} + \frac{a^2\delta^{1-4b}}{(4b-1)(\bar{u}_{L\infty}\rho_L\lambda)^2}\right] + [\gamma(\theta)\cos\theta - \gamma(0)] + \frac{\rho_L g\delta^2}{2g_c} + \left(0{\cdot}416\frac{\delta}{d_e}\right)^{\frac{1}{2}}\tau_i\delta \qquad (29)$$

for the constant velocity profile. Thus for both profiles the film deceleration is zero and the shear force, $F_S = 0$.

The solutions of these equations at the test conditions described in Section 3.1 are listed in Table 2 along with the pertinent physical properties and the constants a and b.

Note that the surface force, F_γ, lies in the range $-0{\cdot}00064$ lb/ft (for $\theta = 0$) to $-0{\cdot}00186$ lb/ft (for $\theta = 180$) and is several orders of magnitude greater than F_E, F_B and F_D. Thus the resulting force is upstream and contrary to our assumption that $\bar{u}_{LE} = \bar{u}_{L\infty}$, the film is decelerated, that is, $\bar{u}_{LE}$ must be less than $\bar{u}_{L\infty}$. Now the heat flux is more than adequate to evaporate the film as it arrives and, as a result, the dry patch grows upstream.

3.4.2 *Case* $\bar{u}_{LE} < \bar{u}_{L\infty}$. The appropriate force equations (19) and (20) contain shear and stagnation terms, F_S and F_M, where

$$F_M = \frac{2\rho_L\delta}{3g_c}\left(\bar{u}_{L\infty}^2 - \bar{u}_{LE}^2\right) \qquad (8)$$

and

$$F_S = \tau_i\frac{(l+m)}{2}(1 - \bar{u}_{LE}/\bar{u}_{L\infty}). \qquad (13)$$

In Table 3 these are compared for various percentage decelerations. To estimate F_S I use Murgatroyd's suggestion that l is of the same order of magnitude as the radius of curvature of the dry patch [4] and assume $l = 0{\cdot}023$ ft and $l + m = 0{\cdot}033$ ft. With 1 per cent deceleration, F_M and F_S are several orders of magnitude greater than F_E, F_B and F_D, but much less than F_γ (Table 2), with 10 per cent deceleration F_S is

Table 3. An estimate of stagnation and shear forces on the meniscus of constant or linear velocity profiles. $\bar{u}_{LE} < \bar{u}_{L\infty}$

	$\bar{u}_{LE}$* (ft/s)	$\bar{u}_{L\infty}$ (ft/s)	Deceleration F_M (10^{-5} lb/ft)	F_S (10^{-5} lb/ft)
1%	1	1·01	0·031	3·0
	2	2·02	0·12	6·0
10%	1	1·1	0·32	27
	2	2·2	1·3	54
50%	1	2	4·6	150
	2	4	18	300
80%	1	5	37	240

* These velocities have been used to permit direct comparison with the other force terms.

of the same order of magnitude as F_γ and above 50 per cent deceleration F_S probably exceeds F_γ. Also in this range, F_M rises to significant values.

Although there is no way of calculating the deceleration in this case, Table 4 indicates the range of solutions of the force balance

$$F = F_\gamma + F_S = 0 \qquad (30)$$

i.e. if F_M is assumed negligible.

Inclusion of F_M would serve to reduce the

Table 4. Film deceleration necessary for dry patch stability for range of possible contact angles

θ film-heater contact angle	Deceleration % decrease in film velocity	
	for $\bar{u}_{L\infty} = 1$ ft/s	for $\bar{u}_{L\infty} = 2$ ft/s
0° (imaginary)	13	6
45°	16	8
90°	25	12
180°	37	18

deceleration, and since the maximum deceleration in Table 4 is below the value where, according to Table 3, F_M becomes significant, F_M is negligible in this case. Hence equation (30) can be said to apply.

3.5 *Proposed mechanisms for maintaining a quasi-stable dry patch*

In general the resultant force acting on the meniscus of the film is

$$F = F_\gamma + F_S + F_M \tag{31}$$

where F_γ is given by (14), F_S by (13) and F_M by (8).

Whether a constant or linear velocity profile is assumed in formulating the expression for F_M is of little consequence at the present stage of development.

I have shown in section 3.4 that the downstream shear force is dependent on the deceleration of the film caused by the upstream surface force. When a dry patch is first formed the upstream surface force will decelerate the approaching film and thus cause a downstream shear force. For the test conditions being considered it is shown in Table 4 that for every possible contact angle there is some shear force which will balance the surface force. In general then the shear force and possibly the stagnation force will increase until a force balance is reached and the dry patch becomes quasi-stable. This is a self adjusting process which will maintain a force balance as long as conditions can be found such that $F = F_\gamma + F_S + F_M = 0$. However if for all degrees of deceleration this condition is not satisfied and $F < 0$ even when the film is completely stagnated then the dry patch will move upstream.

Once a quasi-stable dry patch is formed rewetting can only be accomplished by some perturbation of the system such as an increased film flow or droplet deposition rate. Even then the mid-patch temperature will usually exceed the Leidenfrost point and until this is reduced by conduction through the heater surface the advancing film will be thrown off the heater.

Another source of instability in the force balance is the variable width of the dry patch. If there is any tendency for the patch to grow it will first do so in the direction of the smallest opposing force, i.e. by widening. This will cause greater deceleration at the vertex and an increase in F_S and F_M. As the patch widens to encircle the heater, either the heat flux and nucleation at the film boundary must be sufficient to evaporate and eject the entire film flow or the film will slowly rewet the patch.

Examination of the surface force reveals an additional stabilizing effect. Phillips and Riddiford [12] report that for advancing or receding films of water in a siliconed glass/water vapour system the advancing contact angle θ_A is greater than the static value by 10°, and the receding angle θ_R is less than the static value by 10°. Since the static contact angle usually lies midway between θ_A and θ_R, this discounts the direct use

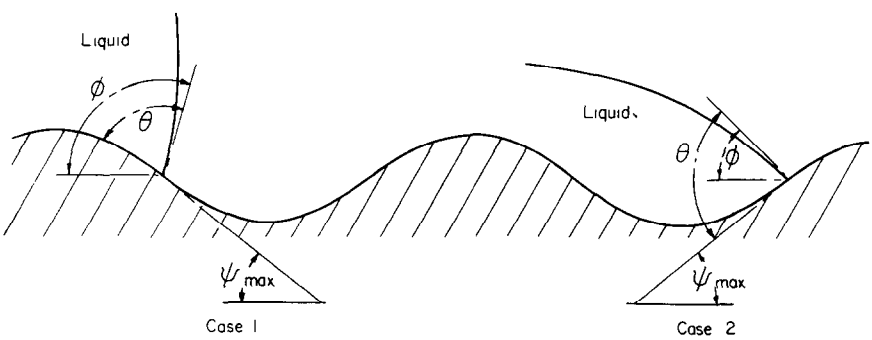

FIG. 8. Effective contact angles with sinusoidal surface roughness.

of a statically measured contact angle for application to dry patch stability.

Shuttleworth and Bailey [13] have studied this question of the effective value of θ in more detail. They argue that for the sinusoidally roughened surface of Fig. 8 the true contact angle is less or greater than the effective contact angle, ϕ_E, according to whether the gradient of the solid at the line of contact is the same as or opposite to that of the liquid surface (Fig. 8, cases 1 and 2 respectively).

It can be seen that for spreading liquid (case 1), the triple interface would move from one ridge to the next, θ decreasing each time, and would come to rest when θ decreased to its equilibrium value, θ_E. The effective equilibrium angle, ϕ_E, would then be

$$\phi_E = \theta_E + \varphi_{max}. \tag{32}$$

Similarly, a receding film would come to rest when

$$\phi_E = \theta_E - \varphi_{max} \text{ (case 2)}. \tag{33}$$

The hysterises in the measured contact angle would therefore be $2\varphi_{max}$.

Equations (32) and (33) will not apply in cases where θ_E or the roughness are such that the film surface defined by them intersects the next ridge. In such cases the advance or recession of the liquid will continue, coming to rest at the first position for which the liquid surface clears the top of the next ridge. For the advancing liquid this will be when

$$\phi_E = \theta_E + \varphi_E \tag{34}$$

and for the receding liquid when

$$\phi_E = \theta_E - \varphi_E \tag{35}$$

where φ_E is the gradient of the groove at the triple interface and is less than φ_{max}.

This explanation accounts for Phillips and Riddiford's results and justifies some experimenters' method of averaging θ_A and θ_R to obtain a best value of contact angle. Deviation from this idealized roughness will lead to modification of equations (32)–(35), but for any given case the deviation of ϕ_E from θ_E is expected to be the same whether measured or an advancing or a receding film.

These ideas may be applied to the contact angle at the vertex of a dry patch, where ϕ_E is the effective value of θ used in the force balance. Assuming sinusoidal roughness with the grooves cut across the heater surface at right angles to the flow direction, I conclude that the advancing film will experience a larger upstream surface force

$$F_{\gamma.A} = \gamma(\theta_E + \varphi_{max}) \cos(\theta_E + \varphi_{max}) - \gamma(0) \tag{36}$$

while the receding film will experience a smaller upstream force

$$F_{\gamma.R} = \gamma(\theta_E - \varphi_{max}) \cos(\theta_E - \varphi_{max}) - \gamma(0) \tag{37}$$

than would be the case for a smooth surface. This provides another possible explanation for the stable existence of a dry patch: as the differential shear force F_S fluctuates the film might oscillate between advancing and receding positions. In the advancing position the larger surface force (36) would come into play to prevent the advance; in the receding position the small surface force (37) would come into play and tend to limit the recession. Hence this additional stabilizing phenomenon associated with surface roughness may reinforce the mechanisms discussed above.

In the special case that θ_E and the roughness result in the film surface intersecting the next ridge there will be no equilibrium surface force until the film has advanced or receded to the point where (34) and (35) hold. This implies an instability in the dry patch boundary which will probably lead to rewetting.

Although some workers have reported on the influence of surface roughness on "burnout" [14–16] the results are inconclusive: some workers found no effect, others found a small inverse relationship. Moreover, these results do not necessarily relate to dry patch stability.

4. DISCUSSION AND CONCLUSIONS

From a detailed analysis of the heat transfer

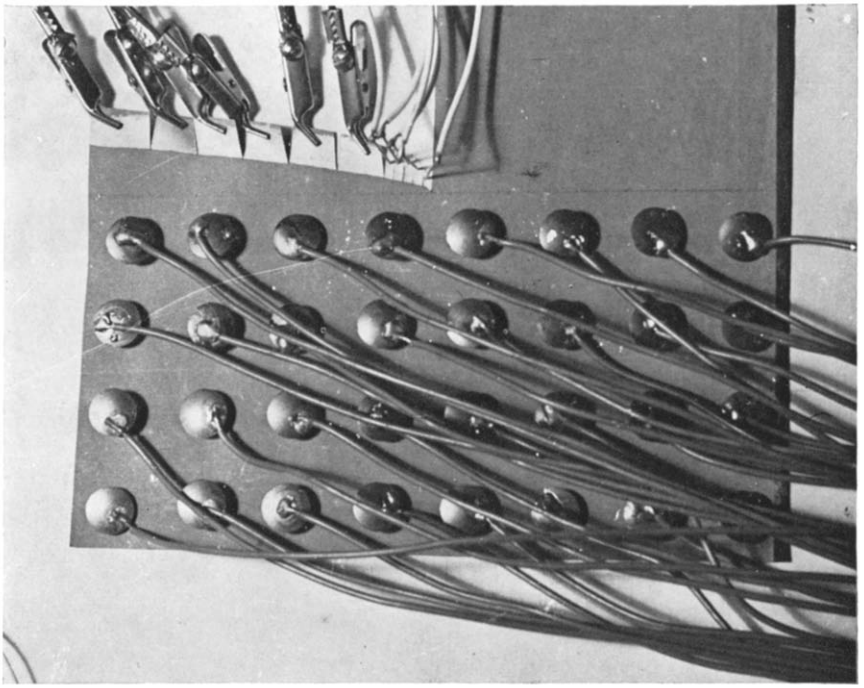

FIG. 9. Electric analogue of ohmically heated wall with dry patch. There are 16 point heat sources per 'square-wall thickness' in a heater length of one wall thickness to either side of triple interface. The liquid film has been shaped at upper left to equate heat of film evaporation to measured heat flux.

[*facing page* 1146]

in the region of the upstream boundary of a dry patch I find that only the differential shear, the stagnation force and the surface force are significant. The resultant axial force on the meniscus of the central stream line of the upstream film is

$$F = \frac{2\rho_L\delta}{3g_c}(\bar{u}_{L\infty}^2 - \bar{u}_{LE}^2) + \tau_i\frac{l+m}{2}(1-\bar{u}_{LE}/\bar{u}_{L\infty}) - [\gamma(0)-\gamma(\theta)\cos\theta].$$

Judging by the relative orders of magnitude of the other forces, this conclusion applies over a wide range of dryout conditions.* At the onset of dryout the upstream surface force causes a deceleration of the film which in turn causes an increase in the downstream shear and stagnation forces. If, over the range of 0–100 per cent deceleration there are conditions for which $F = 0$, the dry patch will be stable. If, on the other hand $F < 0$ for all values of deceleration the patch will spread upstream. Rewetting will occur only as the result of a perturbation in some flow parameter.

There are two additional factors which affect dry patch stability: (1) a tendency for a patch to widen can lead to rewetting; (2) a regular circumferential roughness of the heater wall may result in two surface forces—a larger one which tends to hold back an advancing film, and a smaller one which tends to reduce the force on a receding film. This could result in the film oscillating between advancing and receding positions.

Since my approach was, in part, suggested by Staub and Zuber's (S & Z) earlier paper [5] it is useful to compare it with their later ideas presented in [6]: S & Z considered the stagnation force F_M, the surface force F_γ, and the vapour thrust F_E. They evaluated F_M, assuming that all the film is brought to rest, although the existence of F_E over the meniscus implies that a portion of the film does not come to rest, but continues to flow across the meniscus. In deriving F_γ and F_E, S & Z assumed the meniscus is wedge shaped, terminating at the dry patch in a plane which meets the heater surface at an angle equal to the contact angle. They assumed the temperature distribution over that plane is the same as the upstream distribution as determined by conduction across the laminar film. F_γ was divided into two terms: the surface tension term and the thermocapillary force due to the nonuniform surface tension over the wedge shaped meniscus.

Although the estimate of film temperature distribution is reasonable, the assumption of a wedge shaped meniscus is far from correct, as shown by the very gradual slopes determined in my analogue studies. As a result, F_E is two orders of magnitude too large, but since it is still much smaller than other forces in the case of water, this does not affect S & Z's result for that case. However it should make an important difference in their liquid metal cases where they find F_E is the largest upstream force. Also, it is important that the distortion in heat flux distribution caused by the dry patch be taken into account, as done in the analogue studies. S & Z assumed uniform heat flux, thus increasing their error in F_E.

The idea of a nonuniform temperature distribution over the meniscus is basic to the derivation of the surface force, F_γ. In deriving F_γ, S & Z assumed that the surface tension is everywhere equal, i.e. no account was taken of the lower value (due to the higher temperature) at the triple interface. This point should seriously affect their conclusion that "with liquid of high wettability the effect of the surface force in maintaining a dry patch will be small since the value of the contact angle θ is close to zero, i.e. $(1 - \cos\theta) \approx 0$;" while $(1 - \cos\theta)$ may be near zero, $[\gamma(0) - \gamma(\theta)\cos\theta]$ may be significantly greater, depending on the interface temperatures at the extremities of the meniscus.

S & Z do not consider the body and drag

* e.g. $0 < \dot{Q}/A < 10^6$ Btu/h ft^2 although this can depend on the type of heater; coolant quality > 10 per cent, all mass fluxes and pressures.

forces, however in this analysis they are found to be insignificant.

Another important difference between our studies is that S & Z have not considered the shear force by the vapour core on the stagnating film; I have found that this is the most significant downstream force.

Of course there remain inadequacies with my approach. Most notable is the uncertainty in the film surface temperature at the triple interface. Also there are several unknown values: the stream lengths l and m, the dynamic contact angle θ and the degree of film stagnation. In addition there are uncertainties regarding the dryout model, such as the effect of droplet deposition and entrainment and the film thickness immediately upstream of the dry patch.

Before this approach can be significantly refined, visual verification must be made of the model, measurements are required of the contact angle, film deceleration and the deceleration distance. Prüger's work on interfacial superheat should be extended to higher heat fluxes and a better estimate made of the upstream film velocity and temperature profiles.

Work along these directions is in progress in the Nuclear Engineering Department, Queen Mary College, University of London, and in the Advance Engineering Branch, Chalk River Nuclear Laboratories, Atomic Energy of Canada Limited, Chalk River, Ontario.

ACKNOWLEDGEMENTS

I am grateful to Professor W. Murgatroyd of Queen Mary College, (now at Imperial College), London, England, for his direction of my PhD. program, during which time most of this work was done. I wish to thank H. C. Chung, D. E. Hartley, G. F. Hewitt, H. A. Kearsey and E. O. Moeck for helpful discussions over several years of preparing this paper, and the Babcock and Wilcox Co. (U.K.) and the British Board of Trade for their generous financial support throughout my stay in Britain. The work has been reviewed and the paper prepared at Atomic Energy of Canada Limited, Chalk River, Ontario.

REFERENCES

1. G. D. McPherson and W. Murgatroyd, Film breakdown and dryout in two-phase annular flow, Paper 92, Vol. III, *3rd Int. Heat Transfer Conf.*, Chicago (1966). Also see author's rebuttal in Vol. VI.
2. D. E. Hartley and W. Murgatroyd, Criteria for the break-up of thin liquid layers flowing isothermally over solid surfaces, *Int. J. Heat Mass Transfer* **7**, 1003 (1964).
3. G. F. Hewitt and P. M. C. Lacey, The breakdown of the liquid film in annular two-phase flow, AERE-R 4303 (1963).
4. W. Murgatroyd, The role of shear and form forces in the stability of a dry patch in two-phase film flow, *Int. J. Heat Mass Transfer* **8**, 297 (1965).
5. F. W. Staub and N. Zuber, A program of two-phase flow investigation, second quarterly report, July–Sept. 1963, GEAP-4367, (Oct. 1963).
6. N. Zuber and F. W. Staub, Stability of dry patches forming in liquid films flowing over heated surfaces, *Int. J. Heat Mass Transfer* **9**, 897 (1966).
7. W. Prüger, Die Verdampfungsgeschwindigkeit der Flüssigkeiten, *Z. Phys.* **115**, 202 (1940).
8. M. Jakob, *Heat Transfer*, Vol. 1, p. 619. John Wiley, New
water–steam flow, PhD thesis, Univ. of London (1966).
9. K. Wieghardt, Increase in the turbulent frictional resistance caused by surface irregularities, M.A.P. Völkenrode VG-129-103 T. Min. of Aviation; Reports and translations R & T 103 (1946).
10. J. G. Collier, Heat transfer and fluid dynamic research as applied to fog cooled power reactors, AECL-1631 (1962).
11. G. D. McPherson, The mechanism of film dryout in water-steam flow, PhD thesis, Univ. of London (1966).
12. M. C. Phillips and A. C. Riddiford, Some observations on dynamic contact angles and relaxing interfaces, *Proc. 4th Int. Congr. Surface Activity*, Brussels (1964).
13. R. Shuttleworth and G. L. Bailey, Discussions, *Faraday Soc.* **3**, 16 (1948).
14. F. E. Tippets, Critical heat fluxes and flow patterns in high pressure boiling water flows, *Trans. ASME* **86**, 12 (1964).
15. I. T. Aladyev, Z. L. Miropol'skiy, V. E. Doroshchuk and M. A. Styrikovitch, Boiling crisis in tubes, Part II-A, *Int. Heat Transfer Conf.*, Boulder, Colo., U.S.A. (1961).
16. E. Janssen, S. Levy and J. A. Kervinen, Investigations of burnout in an internally heated annulus cooled by water at 600 to 1450 psia, *ASME Paper* 63 WA-149, Philadelphia (1963).

APPENDIX

The Triple Interface Temperature

Resistance paper analogues were prepared for the conditions of dryout considered here and applied to the cases of both a directly (ohmically) heated tube and the indirectly heated cladding of a nuclear fuel element. Assumptions concerning the flow distribution and heater surface characteristics are discussed in [1].

Construction of the analogue

Teledeltos resistance paper, type 1/1, lead lacquered,

supplied by Wiggins Teape, England, was used for this study in which the electrical resistance of the paper, the electrical current and potential are analogues, respectively, of thermal resistance, heat flux and temperature.

A completed analogue for the ohmical heating case is shown in Fig. 9.

Drawing pins were pushed through the paper to introduce point sources of current evenly distributed throughout the paper representing the wall. Results expected from an infinity of point sources were estimated by comparing the results of analogues using, in turn, 1, 4 and 16 point sources per square wall thickness.

Equivalent lengths of resistance paper were selected to represent the thermal resistance of the wall, liquid film and water–vapour interface. The thickness first selected to represent the liquid film was based on the calculated mean heat transfer coefficient, h_L. A conducting strip adjacent to the film and representing the bulk vapour temperature was divided as shown to permit measurement of the current (i.e. heat flux) from each division. Thus the corresponding quantity of evaporated water and the resultant reduction in film thickness could be calculated. The film thickness was adjusted accordingly with conducting paint and the currents to the drawing pins again equalized. The analogue was considered complete when, with equal currents to the drawing pins (i.e. even ohmic heating in the wall) the local change in film thickness was equal to the evaporation loss due to the local heat flux.

Results

Separate analogues were constructed assuming mean film velocities of 1 and 2 ft/s and for both directly (ohmic) heated and indirectly (nuclear) heated walls from 6 to 80 mils thick 304 stainless steel or 4–55 mils thick Zircaloy. Potentials were measured along the analogue heater surface and converted to temperatures. A small effect of wall thickness in nuclear heaters is shown in Fig. 10 and no significant difference between ohmic and nuclear heater walls is shown in Fig. 11, except for the case of a steel with an exceptionally high temperature coefficient of resistivity.

The higher film velocity leads to a lower heater surface temperature upstream of the interface but has no effect at and downstream of the triple interface. The film thickness results and various implications of these measurements are

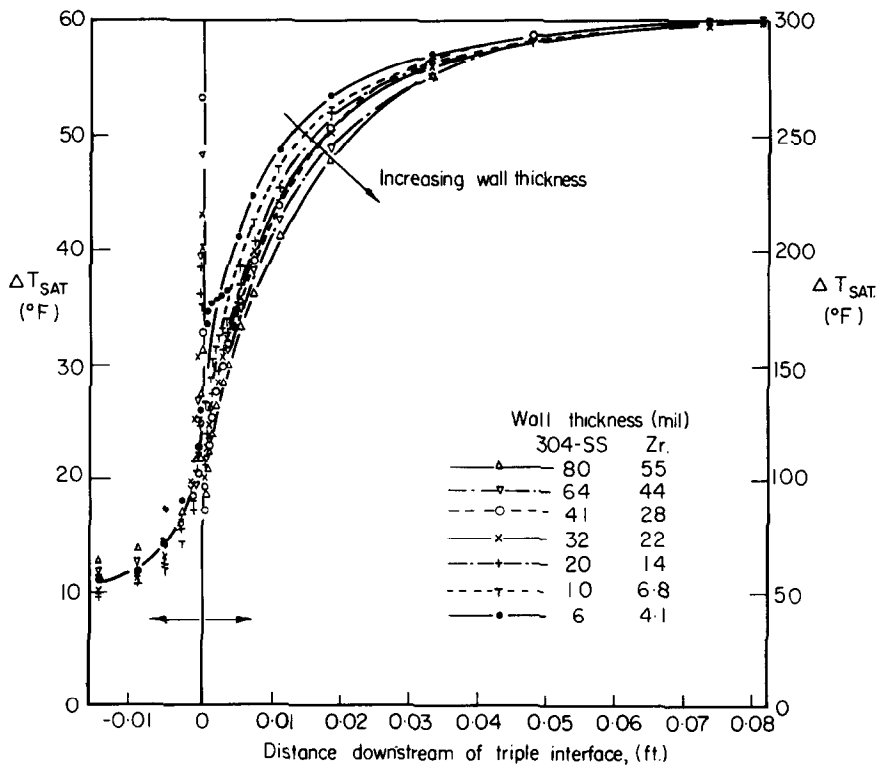

FIG. 10. Surface temperature distribution for nuclear heater with cladding of different thicknesses. Film velocity = 1 ft/s.

discussed in [1] and [11]. For the dryout conditions considered in this paper (64 mil 304 stainless steel, ohmically heated wall, Fig. 11) the triple interface temperature above saturation is taken as the mean of the values 48 F°, measured just upstream, and 100 F°, measured just downstream. For all cases considered in the analogue study, the value of this mean lies between 67 and 95 F°.

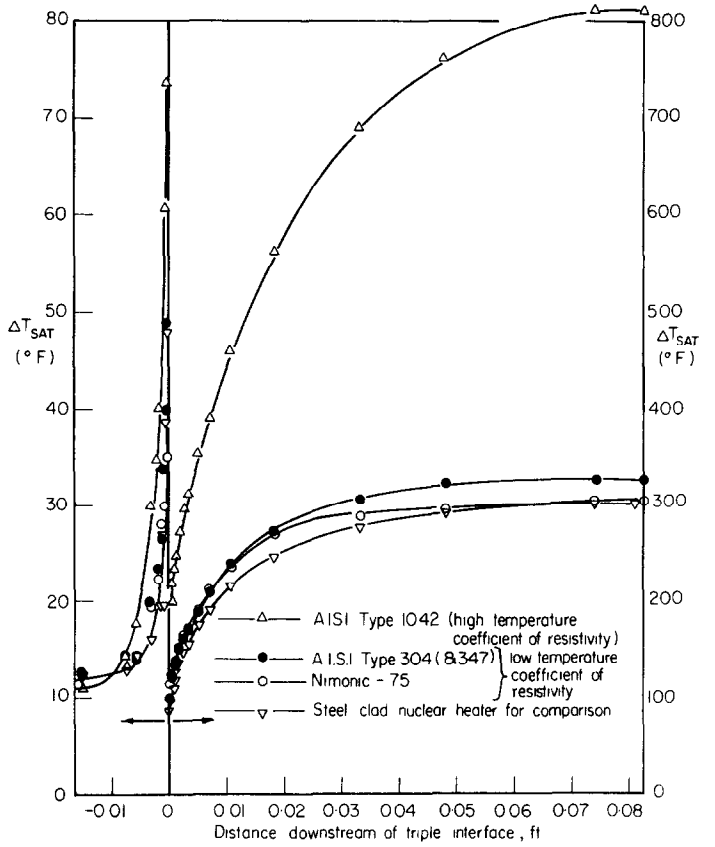

FIG. 11. Surface temperature distribution for 64 mil wall ohmic heaters of different materials.

STABILITÉ AXIALE DE LA TACHE SÈCHE FORMÉE DANS L'ASSÈCHEMENT D'UN ÉCOULEMENT DIPHASIQUE ANNULAIRE

Résumé—Dans le refroidissement d'un combustible nucléaire par des mélanges diphasiques eau-vapeur, la formation d'une tache sèche (assèchement) sur le combustible peut conduire à des températures inacceptables de l'enveloppe et du combustible. L'assèchement est commencé par la nucléation ou par les forces thermocapillaires dans le film liquide qui normalement s'écoule sur la surface chauffée ou bien par épuisement du film. Selon le bilan des forces sur le sommet amont ou le point d'arrêt de la tache sèche, la tache peut être quasi-stable ou transitoire, croissant en amont ou se remouillant.

Les forces considérées sont:

— la poussée de la vapeur quittant la surface,
— la force d'arrêt ou de décélération sur le film en amont du point d'arrêt,
— la tension superficielle au voisinage du point d'arrêt,
— le cisaillement de la vapeur à l'interface film-vapeur,
— la charge hydrostatique dans le film liquide,
— la traînée sur le petit ressaut du film.

La distance en amont de la frontière de la tache sèche sur laquelle ces forces sont effectives est divisée entre la distance sur laquelle le film décélère et est dévié sans changement d'épaisseur et la distance sur laquelle l'évaporation réduit l'épaisseur à zéro.

Les détails suivants sont pris en compte dans l'analyse:

- le profil de vitesses du film,
- la réduction de la force d'arrêt due à l'écoulement d'évaporation,
- les distributions de températures et de flux de chaleur sur la surface chauffante et à travers le film,
- la forme du film.

Les forces sont évaluées pour des conditions d'assèchement typiques. L'interprétation des résultats suggère que pour la stabilité de la tache sèche, la force de cisaillement doit être égale à la force superficielle. Des mécanismes sont proposés par lesquels ces forces peuvent maintenir un bilan quasi-stable. Des comparaisons sont faites avec une méthode semblable employée par Zuber et l'on remarque quelques différences importantes.

AXIALE STABILITÄT DER TROCKENFLECKE INFOLGE VON AUSTROCKNUNG EINER ZWEIPHASEN-RINGSTRÖMUNG

Zusammenfassung—Bei Kühlung von Kernbrennstäben durch ein Wasser-Dampf-Gemisch kann die Entstehung von Trockenflecken (dryout) zu unzulässig hohen Temperaturen im Brennstab und in der Hülle führen. Austrocknung kann entstehen durch Kern- oder Thermokapillarkräfte in dem, normalerweise über die Heizfläche strömenden Flüssigkeitsfilm, oder durch Filmaustrocknung. Abhängig von der Kräftebilanz im stromaufwärts gelegenen Scheitel oder Staupunkt des Trockenflecks kann der Fleck quasistationär oder instationär sein, stromaufwärts wachsen oder durch Benetzung verschwinden. Die betrachteten Kräfte sind:

— Schub des die Filmoberfläche verlassenden Dampfes
— Verzögerungskräfte im stromaufwärts gelegenen Staupunkt
— Oberflächenspannung in der Nähe des Staupunkts
— Schub des Dampfes an der Phasengrenze Flüssigkeit-Dampf
— Hydrostatischer Druck des Flüssigkeitsfilms
— Widerstand der kleinen Stufe im Film.

Die stromaufwärts gelegene Entfernung der Trockenfleckgrenzen an der diese Kräfte wirken, wird aufgeteilt in eine Länge auf der der Film verzögert und ohne Änderung seiner Dicke abgelenkt wird und eine Länge auf der durch Verdampfung die Filmschichtdicke zu Null wird.

ОСЕВАЯ СТАБИЛЬНОСТЬ СУХОГО ПЯТНА, ОБРАЗОВАННОГО ПРИ ОБТЕКАНИИ ТВЭЛ КОЛЬЦЕВЫМ ДВУХФАЗНЫМ ПОТОКОМ

Аннотация—При охлаждении ТВЭЛ двухфазной смесью вода-пар образование сухого участка на ТВЭЛ может привести к недопустимо высокой температуре оболочки и топлива. Высыхание вызывается образованием пузырьков или термокапиллярными силами в пленке жидкости, обычно текущей по нагретой поверхности, или исчезновением пленки. В зависимости от баланса сил в критической точке набегания на сухой участок этот участок может быть квази-стабильным или нестабильным, растущим вверх по течению или вновь увлажняющимся.

Рассмотрены следующие силы:—напор пара, покидающего поверхностную плёнку;
—сила торможения или замедления плёнки вверх по течению от критической точки; сила трения пара на поверхности раедела пленка- пар;
—гидростатический напор от жидкой плёнки;
—натяжение на небольшом уступе в плёнке.

Расстояние по течению от границы сухого участка, на котором действуют эти силы, делится на две части: первую, где пленка замедляется и смещается без изменения толщины, и вторую, где из-за испарения жидкости толщина плёнки уменьшается до нуля. При анализе во внимание принимались следующие детали:
—профиль скорости плёнки;
—ослабление силы торможения за счёт испарения;
—распределение температуры и теплового потока по поверхности нагревателя и в плёнке;
—форма плёнки.

Силы оценивались для типичных условий высыхания. В результате анализа данных предположено, что для стабильности сухого участка сдвиговая сила должна быть равна поверхностной силе. Предложены механизмы, благодаря которым эти силы могут поддерживать квазистабильное равновесие. Проводится сравнение с аналогичным решением Зубера и отмечены некоторые важные различия.